JOURNAL OF MOLECULAR SPECTROSCOPY **184,** 186–201 (1997)
ARTICLE NO. MS977301

Laser and Fourier Transform Emission Spectroscopy of the $G^4\Phi - X^4\Phi$ System of TiF

R. S. Ram,* J. R. D. Peers,† Ying Teng,† A. G. Adam,† A. Muntianu,‡ P. F. Bernath,*,‡ and S. P. Davis§

*Department of Chemistry, University of Arizona, Tucson, Arizona 85719; †Department of Chemistry, University of New Brunswick, Frederiction, New Brunswick, Canada E3B 6E2; ‡Department of Chemistry, University of Waterloo, Waterloo, Ontario, Canada N2L 3G1; and §Department of Physics, University of California, Berkeley, California 94720

Received November 25, 1997; in revised form March 11, 1997

The emission spectrum of the $G^4\Phi - X^4\Phi$ transition of TiF has been observed in the region 13 500–16 000 cm^{-1} using a Fourier transform spectrometer (FTS), as well as by laser excitation spectroscopy. In the FTS experiments the bands were excited in a carbon tube furnace by the reaction of titanium metal vapor with CF_4 at a temperature of about 2300°C. In the laser experiments the TiF molecules were produced by laser vaporization of a Ti rod followed by reaction with SF_6 using a pulsed supersonic jet source. Three groups of bands with high-wavenumber subband heads at 14 388, 15 033, and 15 576 cm^{-1} have been assigned as 0–1, 0–0, and 1–0 vibrational bands of the $G^4\Phi - X^4\Phi$ transition, respectively. Each vibrational band consists of four subbands assigned as $^4\Phi_{3/2} - {}^4\Phi_{3/2}$, $^4\Phi_{5/2} - {}^4\Phi_{5/2}$, $^4\Phi_{7/2} - {}^4\Phi_{7/2}$, and $^4\Phi_{9/2} - {}^4\Phi_{9/2}$. A rotational analysis has been performed and molecular constants for the ground and excited states have been extracted using the combined FTS and laser excitation measurements. The correspondence between the electronic states of TiF, TiH, and Ti^+ has also been discussed.

INTRODUCTION

Transition metal-containing molecules are of current interest because of their importance in astrophysics (*1–3*) and catalysis (*4, 5*). Many theoretical calculations have been carried out, often with the goal of understanding the nature of metal–ligand interactions (*6–8*). These molecules are also of importance in high-temperature chemistry.

In general the electronic spectra of diatomic molecules containing transition elements are very complex. Many transition metal elements have open *d*-shells which results in a high density of electronic states, and these states often have high multiplicity and large orbital angular momenta. The spectra are further complicated by spin–orbit interactions and perturbations between the close-lying electronic states. The analysis of the spectra of transition metal-containing molecules, however, provides valuable information about chemical bond formation and molecular structure. Surprisingly, the spectroscopic properties of many transition metal halides are poorly known experimentally, particularly in comparison with the corresponding oxides and hydrides.

The spectra of diatomic molecules containing 3*d* transition elements are prominent in the spectra of cool stars and sunspots (*2, 3, 9–13*). Titanium-containing molecules are particularly important because Ti has a high cosmic abundance. The presence of TiO and TiH has been well established in the atmospheres of cool stars. For example, TiO has been identified in the spectra of M-type stars (*2, 3, 9*) and sunspots (*10–12*) while TiH has been observed in the spectra of M-type stars (*13*). The recent observation of AlF in the atmosphere of a carbon star (*14, 15*) and the presence of HF in numerous red giant stars (*16*) also strengthen the possibility that transition metal fluorides such as TiF, VF, and CrF may also be found. A positive identification of transition metal fluorides could provide a direct estimate of the fluorine abundance in stars.

To date only limited spectroscopic information is available on the halides of titanium. There are several low-resolution studies of the TiF (*17, 18*), TiCl (*19–21*), TiBr (*22, 23*), and TiI (*24*) molecules. The spectra of these molecules have been investigated in the visible region and a $^4\Pi - X^4\Sigma^-$ transition has been tentatively identified between 380 and 440 nm. In particular there are two independent analyses of TiF bands in the region 380–440 nm. In one study Diebner and Kay (*17*) observed the absorption spectra of TiF between 390 and 410 nm and proposed a ground state vibrational frequency of 593 cm^{-1}, while in another study Chatalic *et al.* (*18*) obtained the same bands in emission and proposed a different vibrational assignment with a ground state vibrational frequency of 607.1 cm^{-1}. Neither of these two values for the vibrational frequency turn out to be correct. In these low-resolution studies the bands were classified into four subbands, namely $^4\Pi_{-1/2} - {}^4\Sigma^-$, $^4\Pi_{1/2} - {}^4\Sigma^-$, $^4\Pi_{3/2} - {}^4\Sigma^-$, and $^4\Pi_{5/2} - {}^4\Sigma^-$.

The assignment of a $^4\Sigma^-$ ground state for TiF (*17, 18*) was based on a primitive theoretical calculation by Carlson and Moser (*25*) for the isoelectronic VO molecule. However, the $^4\Pi - {}^4\Sigma^-$ assignment for this transition has been

0022-2852/97 $25.00

questioned by Shenyavskaya and Dubov (*26*) for TiF and by Phillips and Davis (*27*) for TiCl. Rotational analysis of some of the TiF bands previously assigned to the $^4\Pi-^4\Sigma^-$ transition (*17, 18*) was obtained by Shenyavskaya and Dubov (*26*), who reassigned them as $^2\Phi-^2\Delta$ and $^2\Delta-^2\Delta$ transitions. In another study Phillips and Davis (*27*) rotationally analyzed a few visible bands of TiCl and also assigned them to a $^2\Phi-^2\Delta$ transition.

In our previous studies of transition metal fluorides (*28, 29*) and hydrides (*30, 31*) we have noticed that there is a one-to-one correspondence between the low-lying electronic states of transition metal hydrides and fluorides. The correspondence between hydrides and fluorides is well known in spectroscopy although it has not been much exploited. A comparison of the available data for TiF (*17, 18, 26*) with those for TiH (*32–35*) suggests that the assignment of a $^4\Sigma^-$ or a $^2\Delta$ ground state for TiF is unlikely since TiH is known to have a $^4\Phi$ ground state.

There are only a limited number of theoretical studies of titanium monohalide molecules (*36*). A crude prediction of the low-lying electronic states of TiF was obtained by Cambi (*36*) using the semiempirical computational method devised by Fenske *et al.* (*37*). This calculation predicted a $^4\Sigma^-$ ground state followed by $^2\Delta$, $^4\Phi$, and $^4\Pi$ states at higher energy. Recently, an ab initio study of TiF has been carried out by Harrison (*38*), who has calculated the spectroscopic properties of a number of doublet and quartet states. This work predicts a $^4\Phi$ ground state for TiF consistent with the TiH results. According to Harrison's calculations there is a low-lying $^4\Sigma^-$ state which is about 0.1 eV above the $X^4\Phi$ state. This calculation also predicts that the lowest-lying doublet state is the $^2\Phi$ state which lies about 0.65 eV above the ground $^4\Phi$ state.

A mass spectroscopic study of TiF along with TiF_2 and TiF_3 has been carried out by Zmbov and Margrave (*39*). This work establishes the relative stability of TiF_2 and TiF_3 through equilibrium measurements and provides an estimate of 136 ± 8 kcal/mole for the dissociation energy of TiF. The strong Ti–F bond improves the chances of forming TiF in stellar atmospheres, particularly in AGB stars. A Ti–F bond length of 1.754 Å has been obtained for TiF_4 from an electron diffraction experiment by Petrov *et al.* (*40*). Several unsuccessful attempts were made to record the ESR spectrum of TiF in rare gas matrices by DeVore *et al.* (*41*) and they concluded that the ground state of TiF was most probably not a $^4\Sigma^-$ as assigned previously (*17, 18*).

In the present paper we report on the observation of a $^4\Phi-^4\Phi$ transition of TiF in the region 14 000–16 000 cm^{-1}. This transition has been assigned as the $G^4\Phi-X^4\Phi$ transition based on the recent theoretical predictions of Harrison (*38*) and on the experimental and theoretical information available for the TiH molecule (*32–35*). The rotational analysis of the 0–1, 0–0, and 1–0 bands of this transition has been obtained, providing the first high-resolution spectroscopic data for all four spin components of the ground state of TiF. Many bands with complex structure remain to be analyzed in the region 4000–14 000 cm^{-1}. The observation of the $G^4\Phi-X^4\Phi$ transition in laser excitation experiments using a molecular beam source also confirms that the lower state of this transition is most probably the ground state of TiF.

EXPERIMENTAL DETAILS

The TiF bands have been observed in two different experiments: Fourier transform emission spectroscopy at the National Solar Observatory in Tucson, Arizona, and laser vaporization spectroscopy at the University of New Brunswick, Canada. The details for each experiment will be provided separately.

1. Fourier Transform Emission Spectroscopy

The emission spectra of TiF were produced by the reaction of titanium metal vapor with CF_4 in a high-temperature carbon tube furnace at a temperature of about 2300°C. The initial experiment was intended to record improved spectra of the 1-μm system of TiH which has been previously recorded by two of the authors using a hollow cathode source (*42*). In this experiment about 90 Torr H_2 was added along with about 100 Torr He as a buffer gas. The TiH bands were observed very weakly, and we decided to search for the analogous transition of TiF using the same experimental conditions but using CF_4 instead of H_2. When a small amount of CF_4 was added, numerous strong bands were observed from 4000 to 16 000 cm^{-1}. The bands in the region 4000–13 000 cm^{-1} are very complex in appearance because of overlapping from neighboring bands. Some of these bands probably do not belong to TiF since the intervals between the rotational lines are too large for TiF. The weaker bands observed in the region 13 500–16 000 cm^{-1}, however, are relatively free from overlapping and were readily identified as belonging to a single transition with the 0–0 band near 15 033 cm^{-1}. This transition has been named the $G^4\Phi-X^4\Phi$ transition by comparing the TiF and TiH energy level diagrams as will be discussed below.

The emission from the furnace was focused onto the 8-mm entrance aperture of the 1-m Fourier transform spectrometer of the National Solar Observatory at Kitt Peak. The spectra were recorded using silicon photodiode detectors and RG 645 filters at a resolution of 0.02 cm^{-1}. A total of six scans were coadded in about 30 min of integration and the spectra had a signal-to-noise ratio of about 15:1.

The spectral line positions were determined using a data reduction program called PC-DECOMP developed by J. Brault. The peak positions were determined by fitting a Voigt lineshape function to each line. The present spectra were

calibrated using the laser measurements (described in the following section) of a number of lines of the 0–0 and 1–0 bands of TiF. The molecular lines appear with a typical width of 0.07 cm^{-1} and the line positions are expected to be accurate to about ± 0.005 cm^{-1}. However, since there is considerable overlapping and blending caused by the presence of different subbands in the same region, the error in the measurement of blended and weak lines is expected to be somewhat higher.

2. Laser Excitation Spectroscopy

The apparatus used to create the TiF molecule in the molecular beam work has been described previously (*43, 44*); however, some details pertinent to this work will be given. A titanium target in the form of a slowly rotating and translating rod was ablated by about 6 mJ of 355-nm radiation from a Nd:YAG laser. At the same time, a gas mixture of 0.8% SF_6 seeded in helium was passed from a pulsed molecular beam valve into the ablation region. Vaporized titanium was entrained by the gas mixture and then expanded through a short expansion channel into a vacuum chamber, producing a molecular jet.

TiF molecules are formed through reaction of the hot Ti atoms with SF_6 and its decomposition products during the expansion process. About 5 cm downstream from the nozzle orifice, the molecules were probed with a tunable dye laser. For low-resolution studies the laser was a Lumonics pulsed dye laser, while for high-resolution spectra the laser was a Coherent 699-29 ''Autoscan'' cw ring dye laser. Laser-induced fluorescence was collected orthogonally to both the molecular beam and the probe laser and imaged on a 0.25-m monochromator. Light passing through the monochromator was detected by a cooled photomultiplier tube. The signal was amplified, integrated, and sent either to a chart recorder or to the computer controlling the Autoscan laser system. DCM dye was used in both lasers to record spectra for the 0–0 and 1–0 bands of the $G^4\Phi$–$X^4\Phi$ transition. Typical linewidths were about 0.1 cm^{-1} for the low-resolution scans, limited by the laser linewidth, and about 180 MHz for the high-resolution scans where the limitation was residual Doppler broadening in the molecular beam. The line positions were measured using the Autoscan system, which has a specified absolute frequency accuracy of ± 200 MHz and a precision of ± 60 MHz. Calibration of the Autoscan system was maintained by recording a section of the I_2 spectrum and comparing the line positions with the values published in the I_2 atlas (*45*).

DESCRIPTION OF OBSERVED BANDS

1. Fourier Transform Emission Spectroscopy

The TiF bands assigned to the $G^4\Phi$–$X^4\Phi$ transition are located in the spectral region 13 000 to 16 000 cm^{-1}. In this region three groups of bands have been observed with the high-wavenumber R heads at 14 383, 15 033, and 15 576 cm^{-1} (Fig. 1), assigned as the 0–1, 0–0, and 1–0 vibrational bands, respectively. The next members in the $\Delta v = -1$, 0, 1 sequences (the 1–2, 1–1, and 2–1 bands) could not be identified because of their weaker intensity and overlapping from the stronger main bands. The 0–2 and 2–0 bands could not be identified in our spectra because of their very weak intensity. In the 0–1 and 1–2 band region there is a weak head-like structure near 14 150 cm^{-1} but this band probably belongs to another transition. To lower wavenumbers there are additional weak heads near 13 230, 13 600, and 14 690 cm^{-1}, which may be associated with the 14 150 cm^{-1} band. All of these bands are degraded toward lower wavenumbers (red degraded) and have weak R heads.

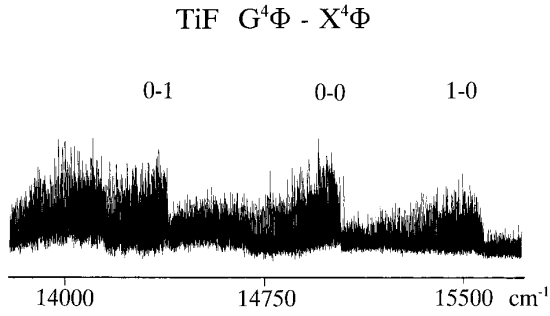

FIG. 1. A compressed portion of the low-resolution spectrum of the $G^4\Phi$–$X^4\Phi$ transition of TiF.

The structure of each of these bands is very complex because of overlapping from different subbands. A Hund's case (a) $^4\Phi$–$^4\Phi$ transition consists of four main subbands $^4\Phi_{3/2}$–$^4\Phi_{3/2}$, $^4\Phi_{5/2}$–$^4\Phi_{5/2}$, $^4\Phi_{7/2}$–$^4\Phi_{7/2}$, and $^4\Phi_{9/2}$–$^4\Phi_{9/2}$, which are separated by three times the difference between the spin–orbit coupling constants of the upper and lower electronic states. The Ω-assignment in different subbands is confirmed by the B_{eff} values in the different spin components with $B(^4\Phi_{9/2}) > B(^4\Phi_{7/2}) > B(^4\Phi_{5/2}) > B(^4\Phi_{3/2})$ as expected for a regular $^4\Phi$ state (see Discussion). In contrast to the laser experiments, no first lines were seen in the FTS experiments.

A schematic energy level diagram of the $^4\Phi$–$^4\Phi$ transition is presented in Fig. 2. The subband order in each vibrational band is $^4\Phi_{9/2}$–$^4\Phi_{9/2}$, $^4\Phi_{7/2}$–$^4\Phi_{7/2}$, $^4\Phi_{5/2}$–$^4\Phi_{5/2}$, and $^4\Phi_{3/2}$–$^4\Phi_{3/2}$ in order of increasing wavenumbers. It was noticed that the 0–0 and 0–1 bands of the $^4\Phi_{5/2}$–$^4\Phi_{5/2}$ and $^4\Phi_{3/2}$–$^4\Phi_{3/2}$ subbands lie very close to each other, separated by only 0.18 cm^{-1}. This is a coincidence since all four heads were found to be well separated in the 1–0 band. Parts of the 0–0 and 1–0 bands are presented in Fig. 3 where the heads due to the four subbands in each band have been marked. These observations also suggest that the ground state is a well-behaved $^4\Phi$ state in which all of the four spin

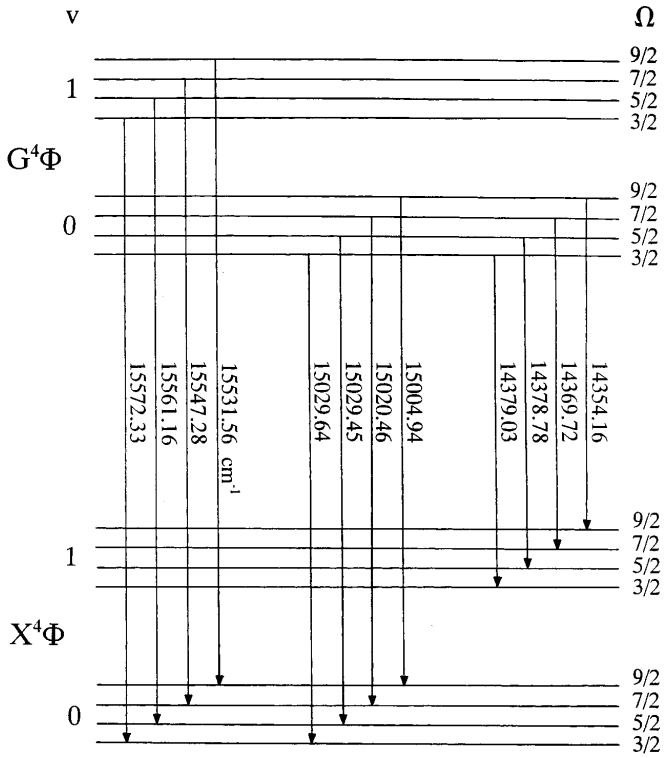

FIG. 2. A schematic energy level diagram of the $G^4\Phi-X^4\Phi$ transition of TiF with arrows marking the observed subbands. The band origins for different subbands are also listed.

components have similar vibrational intervals whereas in the excited state the four spin components have different vibrational intervals. This results in a different subband pattern for the 1–0 band as compared to that in the 0–0 and 0–1 bands. The excited $G^4\Phi$ state is interacting with a close-lying state (or states) not observed in this work.

At first glance the spectra appear very complex and the lines belonging to the high-wavenumber subbands were the only ones to be clearly identified. However, a careful inspection of the spectra using a Loomis–Wood program provided the lines of all four spin components. The structure of each of the four subbands consists of *R* and *P* branches consistent with the $\Delta\Omega = 0$ assignment. No *Q* branches were detected in any of the subbands (in FTS spectra) and no transitions which violate the Hund's case (*a*) selection rule $\Delta\Sigma = 0$ could be identified. This means that we are unable to directly determine any intervals between the spin components from the FTS measurements alone. Ω-doubling is not observed in any of the subbands as expected for a $^4\Phi-^4\Phi$ transition.

The *R* head at 15 033 cm^{-1} has been identified as the 0–0 band of the 3/2–3/2 subband. No Ω-doubling was observed even for the highest *J* values observed. The $v = 0$ vibrational level of the $G^4\Phi_{3/2}$ spin component is perturbed between $J' = 56.5$ and 65.5 and several of the lines in the perturbed region were not definitely identified because of strong overlapping and irregular spacing. In fact in the 0–1 band no rotational lines could be identified for J' values above 56.5. The $v = 1$ vibrational level of the $G^4\Phi_{3/2}$ spin component is also perturbed. In this vibrational level perturbations are found in two regions: the first perturbation is observed at $J' = 21.5$ and the other perturbation is observed at $J' = 31.5$. At this early stage of analysis the source of these perturbations is unclear, although there are many possibilities (e.g., $F^4\Delta$ state).

The subbands with 0–0 heads located at 15 032.8, 15 024.0, and 15 009.5 cm^{-1} have been assigned to the 5/2–5/2, 7/2–7/2, and 9/2–9/2 subbands, respectively. No rotational perturbations have been observed in any of these subbands. The 7/2–7/2 and 9/2–9/2 subbands are weaker in intensity and are strongly overlapped by 3/2–3/2 and 5/2–5/2 subbands. The rotational lines of these subbands were not obvious at first glance and again the use of our Loomis–Wood program was essential in identifying the rotational lines. An expanded portion of the 0–0 band near the *R* heads of the $^4\Phi_{3/2}-^4\Phi_{3/2}$, $^4\Phi_{5/2}-^4\Phi_{5/2}$, and $^4\Phi_{7/2}-^4\Phi_{7/2}$ subbands is presented in Fig. 4.

2. *Laser Excitation Spectroscopy*

Two vibrational bands of the $G^4\Phi-X^4\Phi$ system of TiF were recorded in the molecular beam experiments, the 0–0 and 1–0 bands. An attempt was made to record the 0–1 band but this band showed up only weakly in the pulsed dye laser scans and lies in a region where the DCM dye laser falls off rapidly in laser power. No high-resolution data could be obtained for the 0–1 band.

A comparison between the FTS data and the molecular

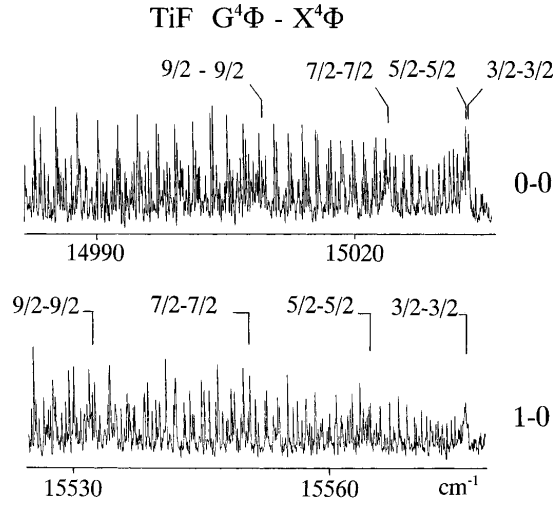

FIG. 3. A portion of the 0–0 and 1–0 bands of the $G^4\Phi-X^4\Phi$ system of TiF. The *R*-head positions of different subbands have been marked.

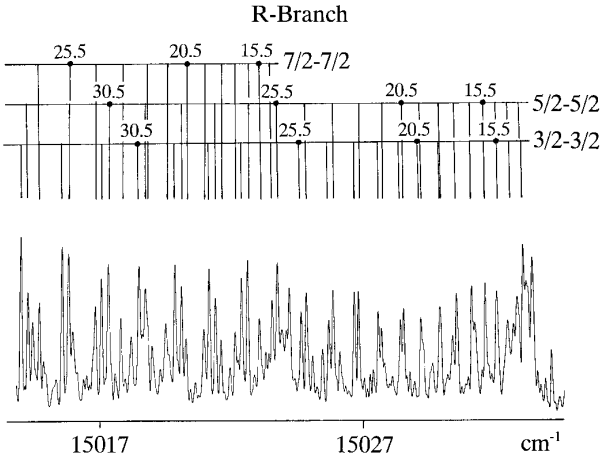

FIG. 4. An expanded portion of the 0–0 band of the $G^4\Phi$–$X^4\Phi$ system of TiF near the R heads of the $^4\Phi_{3/2}$–$^4\Phi_{3/2}$, $^4\Phi_{5/2}$–$^4\Phi_{5/2}$, and $^4\Phi_{7/2}$–$^4\Phi_{7/2}$ subbands.

beam data is given in Figs. 4 and 5. The FTS data for the 0–0 band, Fig. 4, clearly show the problem of overlapping lines from the different subbands. This was not a problem in the molecular beam work, Fig. 5. Even in the closely spaced R-head region of the overlapping 3/2–3/2 and 5/2–5/2 subbands, we were able to resolve the lines. All of the branches could be followed easily from the first lines out to about $J = 20.5$ where the signal becomes too weak. In all, data were recorded for the 3/2–3/2, the 5/2–5/2, and the 7/2–7/2 subbands in both the 0–0 and 1–0 vibrational bands of the $G^4\Phi$–$X^4\Phi$ system. R, P, and Q branches were observed for these subbands.

The transitions for the 9/2–9/2 subband were too weak in intensity to be recorded with the ring laser, presumably because the $X^4\Phi_{9/2}$ spin component lies three spin–orbit intervals above the $X^4\Phi_{3/2}$ spin component and therefore has only a small population in the molecular beam. The same population argument also leads us to believe that the lower $^4\Phi$ electronic state involved in this transition must be the ground state. Given that the transitions from the $X^4\Phi_{9/2}$ spin component and from the $v'' = 1$ level for the ground state (the vibrational spacing is about 650 cm^{-1}) are weak, even in the pulsed dye laser experiments, it is reasonable to assume that a low-lying electronic state such as the $^4\Sigma^-$ state which is calculated to be 0.1 eV (800 cm^{-1}) higher than the $X^4\Phi$ state will not be populated in the molecular beam.

As in the FTS spectra, no lines violating the Hund's case (a) selection rule, $\Delta\Sigma = 0$, could be recorded. However, it was possible to measure the spin–orbit interval between the $X^4\Phi_{3/2}$ and $X^4\Phi_{5/2}$ levels. This was accomplished in a pulsed laser experiment. Narrow slits were used in a small monochromator with a resolution of about ±2 nm. The monochromator was then set to observe fluorescence of the 5/2–5/2 subband R head at 15 032.8 cm^{-1} and the dye laser was scanned to higher wavenumber. In this way, a transition from the $X^4\Phi_{3/2}$ spin component to the $G^4\Phi_{5/2}$ spin component could be observed by monitoring the strong fluorescence back to the $X^4\Phi_{5/2}$ spin component. We were able to observe a signal when the laser was scanned 101.84 cm^{-1} (with an error of perhaps 10 cm^{-1}) higher in wavenumber.

ANALYSIS AND RESULTS

The rotational assignments in the different bands were made by comparing combination differences for the common vibrational levels. Since no transitions involving $\Delta\Sigma \neq 0$ were observed in the FTS spectra, the subbands of different spin components were initially fitted separately using a simple empirical term energy expression (Eq. [1]), even though the lower $^4\Phi$ state obeys Hund's case (a) coupling. The term energy expression for a spin component with no Ω-doubling is

$$F_v(J) = T_v + B_vJ(J+1) - D_v[J(J+1)]^2 + H_v[J(J+1)]^3 + L_v[J(J+1)]^4. \quad [1]$$

The lines from both FTS and laser measurements were ultimately combined and fitted simultaneously. The initial band-by-band fit of different subbands provided similar constants for common vibrational levels, confirming the vibrational assignments. In the final fit, the lines of all of the vibrational bands in each subband were combined and fitted simultaneously. The observed line positions for the different subbands of $G^4\Phi$–$X^4\Phi$ are provided in Table 1. For the transitions

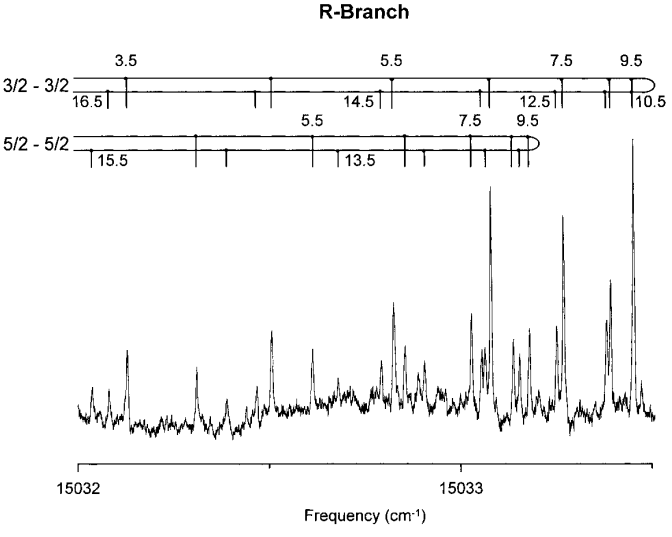

FIG. 5. A portion of the laser excitation spectrum of the 0–0 band near the R heads of the $^4\Phi_{3/2}$–$^4\Phi_{3/2}$ and $^4\Phi_{5/2}$–$^4\Phi_{5/2}$ subbands.

TABLE 1
Observed Line Positions (in cm^{-1}) for the $G^4\Phi - X^4\Phi$ Transition of TiF

A

R- and P-branch lines

$^4\Phi_{3/2}$ - $^4\Phi_{3/2}$ Sub-band

	0-1				0-0				1-0			
J	R(J)	O-C	P(J)	O-C	R(J)	O-C	P(J)	O-C	R(J)	O-C	P(J)	O-C
1.5					15031.180a	-4			15573.863a	5		
2.5					15031.690a	-1	15027.694a	-2	15574.350a	-1		
3.5					15032.130a	-4	15026.809a	1	15574.778a	2	15569.482a	2
4.5					15032.508a	-5	15025.857a	2	15575.133a	-2	15568.515a	0
5.5					15032.830a	0	15024.844a	5	15575.423a	-2	15567.484a	2
6.5					15033.078a	-3	15023.762a	2	15575.650a	2	15566.381a	-0
7.5					15033.269a	-1	15022.627a	9	15575.803a	-1	15565.211a	-2
8.5					15033.393a	-2	15021.409a	-2	15575.891a	-1	15563.987a	9
9.5					15033.453a	-2	15020.139a	-2	15575.912a	-1	15562.672a	-4
10.5					15033.453a	1	15018.807a	-0	15575.864a	-1	15561.304a	-2
11.5			14367.168	8	15033.382a	-2	15017.413a	3	15575.749a	-2	15559.867a	-0
12.5					15033.251a	-1	15015.954a	5	15575.567a	-1	15558.360a	-3
13.5			14364.302	-3	15033.055a	-2	15014.426a	1	15575.322a	4	15556.789a	-2
14.5	14382.764	13	14362.781	-9	15032.797a	0	15012.846a	10	15575.001a	1	15555.147a	-5
15.5	14382.506	1	14361.220	4	15032.470a	-3	15011.183a	-0	15574.634a	19	15553.445a	0
16.5	14382.196	-5	14359.579	-3	15032.082a	-4	15009.470a	3	15574.187a	25	15551.676a	5
17.5	14381.847	10	14357.885	-6	15031.636a	3	15007.690a	3	15573.689a	48	15549.849a	20
18.5	14381.422	9	14356.148	8	15031.128a	12	15005.848a	5	15573.145	91	15547.953a	33
19.5	14380.925	-5	14354.329	-2	15030.551	17	15003.944a	9	15572.675	277	15546.004a	60
20.5	14380.390	2	14352.452	-10	15029.906	18	15001.973a	10	15571.333	-342	15544.006	105
21.5	14379.781	-4	14350.524	-10	15029.177	-1	14999.916	-11	15570.728	-156	15542.073	282
22.5	14379.121	-3	14348.539	-9	15028.402	-1	14997.824	-3	15569.919	-107	15539.270	-343
23.5	14378.387	-14	14346.517	16	15027.562	-0	14995.659	-3	15569.028	-72	15537.206	-162
24.5	14377.602	-18	14344.390	-6	15026.650	-7	14993.435	1	15568.053	-54	15534.944	-113
25.5	14376.768	-10	14342.239	7	15025.680	-7	14991.133	-7	15567.028	-19	15532.573	-105
26.5	14375.863	-13	14340.020	13	15024.640	-12	14988.785	2	15565.934	14	15530.164	-69
27.5	14374.913	-1	14337.708	-15	15023.537	-14	14986.344	-17	15564.795	70	15527.715	-6
28.5	14373.886	-6	14335.365	-16	15022.376	-9	14983.876	2	15563.589	126	15525.152	9
29.5	14372.809	0	14332.971	-7	15021.144	-9	14981.308	-15	15562.441	306	15522.555	58
30.5	14371.677	11	14330.499	-17	15019.848	-9	14978.707	1	15561.375	635	15519.924	139
31.5	14370.472	11	14327.991	-2	15018.476	-18	14976.005	-21	15558.375	-903	15517.300	293
32.5	14369.196	-0	14325.411	0	15017.057	-9	14973.277	-3	15557.216	-534	15514.814	651
33.5	14367.890	19	14322.757	-11	15015.565	-6	14970.466	-4	15555.764	-392	15510.385	-868
34.5	14366.498	14	14320.044	-21	15014.003	-9	14967.590	-4	15554.175	-321	15507.722	-555
35.5	14365.052	16	14317.290	-13	15012.378	-7	14964.650	-3	15552.502	-269	15504.841	-396
36.5	14363.533	6			15010.689	-4	14961.660	14	15550.736	-245	15501.820	-310
37.5	14361.968	11	14311.585	-12	15008.932	-1	14958.573	-1	15548.925	-200	15498.687	-273
38.5	14360.318	-6	14308.633	-20	15007.110	2	14955.449	12	15547.004	-203	15495.465	-260
39.5	14358.641	11	14305.630	-19	15005.216	0	14952.245	10	15545.079	-145	15492.223	-203
40.5	14356.895	20	14302.567	-16	15003.264	7	14948.967	1	15543.023	-156	15488.855	-209
41.5	14355.075	18	14299.450	-7	15001.242	10	14945.632	1	15540.939	-131	15485.484	-155
42.5	14353.157	-20	14296.260	-10	14999.153	14	14942.241	9	15538.783	-118	15482.028	-124
43.5	14351.228	-8	14293.005	-16	14997.000	21	14938.774	9	15536.569	-101	15478.478	-126
44.5	14349.241	10	14289.702	-11	14994.788	36	14935.249	16	15534.337	-43	15474.878	-117
45.5	14347.175	10	14286.333	-8	14992.489	31	14931.652	18	15531.951	-80	15471.238	-87
46.5	14345.042	7	14282.919	10	14990.164	69	14927.987	18	15529.580	-44	15467.525	-72
47.5	14342.858	14	14279.418	3	14987.745	79	14924.267	29	15527.116	-45	15463.722	-89
48.5	14340.611	22	14275.844	-16	14985.253	84	14920.471	31	15524.634	-8	15459.899	-69
49.5	14338.264	-7	14272.248	5	14982.724	120	14916.621	46	15522.072	2	15456.029	-40
50.5	14335.903	13			14980.097	127	14912.715	71	15519.447	1	15452.090	-27
51.5	14333.432	-14			14977.412	144	14908.774	128	15516.770	-2	15448.086	-26
52.5	14330.929	-9			14974.515	17			15514.051	1	15444.046	-10
53.5	14328.367	1			14971.699	39			15511.282	1	15439.952	0
54.5	14325.740	9			14968.806	53	14896.259	11	15508.480	10	15435.808	8
55.5	14323.029	-2			14965.863	87	14892.016	36	15505.621	5	15431.598	-4
56.5					14962.825	94	14887.678	32	15502.738	12	15427.362	-1
57.5					14959.802	184	14883.340	96	15499.786	-14	15423.084	1
58.5					14956.652	217	14878.871	98	15496.838	-3	15418.766	-1
59.5					14953.416	234	14874.381	146	15493.852	-2	15414.421	5
60.5							14869.878	248	15490.833	-10	15410.033	-3
61.5									15487.799	-13	15405.619	-8
62.5									15484.757	-7	15401.186	-10
63.5									15481.708	2	15396.764	19

TABLE 1—*Continued*

$^4\Phi_{3/2}$ - $^4\Phi_{3/2}$ Sub-band

	0-1				0-0				1-0			
J	R(J)	O-C	P(J)	O-C	R(J)	O-C	P(J)	O-C	R(J)	O-C	P(J)	O-C
64.5							14849.863	-661	15478.635	-7	15392.286	7
65.5					14931.870	-335	14845.056	-520				
66.5					14928.280	-184	14840.158	-402			15383.329	4
67.5					14924.522	-130	14835.143	-332				
68.5					14920.673	-98	14830.112	-209				
69.5					14916.738	-80	14824.957	-142				
70.5					14908.648	-53	14819.700	-107				
71.5					14904.465	-71	14814.366	-81				
72.5					14900.274	-27	14808.946	-71				
73.5					14896.021	27	14803.460	-57				
74.5					14891.610	-6	14797.904	-45				
75.5					14887.167	1	14792.269	-41				
76.5					14882.637	-9	14786.576	-27				
77.5					14878.055	1	14780.804	-22				
78.5					14873.382	-8	14774.965	-14				
79.5					14868.665	10	14769.051	-11				
80.5					14863.847	-1	14763.069	-6				
81.5					14858.974	5	14757.033	14				
82.5					14854.016	-3	14750.891	-1				
83.5					14848.994	-2	14744.696	1				
84.5					14843.916	14	14738.437	8				
85.5					14838.735	-1	14732.097	4				
86.5							14725.686	0				
87.5							14719.213	4				
88.5							14712.661	-1				
89.5							14706.028	-17				

$^4\Phi_{5/2}$ - $^4\Phi_{5/2}$ Sub-band

	0-1				0-0				1-0			
2.5					15031.503a	-2			15563.173a	-3		
3.5					15031.946a	4	15026.603a	6	15563.600a	5	15558.284a	2
4.5					15032.312a	-1	15025.641a	8	15563.953a	8	15557.306a	2
5.5					15032.616a	-3	15024.608a	6	15564.224a	-1	15556.254a	-2
6.5					15032.859a	1	15023.505a	-1	15564.433a	-3	15555.133a	-5
7.5					15033.027a	-4	15022.337a	-7	15564.576a	1	15553.952a	1
8.5			14370.648	7	15033.137a	-1	15021.114a	-2	15564.650a	4	15552.692a	-1
9.5			14369.403	8	15033.180a	0	15019.823a	1	15564.650a	3	15551.361a	-6
10.5			14368.098	10	15033.154a	-1	15018.459a	-4	15564.576a	-0	15549.979a	9
11.5			14366.715	-6	15033.063a	-2	15017.033a	-4	15564.433a	-4	15548.502a	-2
12.5	14382.652	-3	14365.313	19	15032.910a	3	15015.545a	-1	15564.224a	-4	15546.974a	7
13.5	14382.506	6			15032.683a	-1			15563.953a	5	15545.357a	-5
14.5	14382.283	-0	14362.243	-12	15032.391a	-4	15012.367a	1	15563.600a	1	15543.685a	-2
15.5	14382.008	1	14360.636	-8	15032.038a	-1	15010.674a	-3	15563.173a	-6	15541.944a	3
16.5	14381.671	3	14358.982	8			15008.931a	9	15562.690a	-0	15540.119a	-7
17.5	14381.275	6	14357.262	21			15007.095a	-6	15562.127a	-3	15538.239a	-3
18.5	14380.817	9	14355.438	-11			15005.214a	-1	15561.499a	-2	15536.268	-20
19.5	14380.291	5	14353.584	-11			15003.263a	1	15560.807a	5		
20.5	14379.706	3	14351.679	-1	15029.267	1	15001.245	1	15560.028	-5	15532.156	-15
21.5			14349.711	6	15028.524	12	14999.153	-7	15559.189	-5	15530.006	-2
22.5	14378.372	20			15027.685	-6	14997.000	-9	15558.292	6	15527.770	-6
23.5	14377.602	18	14345.569	-3	15026.811	7	14994.788	-5	15557.316	9	15525.473	-2
24.5	14376.768	13	14343.404	-9	15025.844	-7	14992.497	-14	15556.265	6	15523.100	-5
25.5	14375.863	-1	14341.204	9	15024.845	14	14990.164	3	15555.146	4	15520.657	-8
26.5	14374.913	2	14338.911	-4	15023.741	-3	14987.745	-2	15553.967	12	15518.158	2
27.5	14373.886	-12	14336.567	-6	15022.609	18	14985.253	-14	15552.700	1	15515.581	4
28.5	14372.809	-13	14334.155	-17	15021.382	12	14982.724	4	15551.375	2	15512.945	14
29.5	14371.677	-8	14331.710	2	15020.095	12	14980.097	-10	15549.992	12	15510.214	-2
30.5	14370.472	-13	14329.198	14	15018.733	4	14977.419	-10	15548.527	10	15507.426	-6
31.5	14369.225	1	14326.603	4	15017.323	14			15547.004	19	15504.584	4

TABLE 1—*Continued*

$^4\Phi_{5/2}$ - $^4\Phi_{5/2}$ Sub-band

	0-1				0-0				1-0			
J	R(J)	O-C	P(J)	O-C	R(J)	O-C	P(J)	O-C	R(J)	O-C	P(J)	O-C
32.5	14367.890	-11	14323.956	3	15015.812	-9			15545.388	3	15501.665	6
33.5	14366.512	-4	14321.276	31	15014.265	-1	14968.982	-12	15543.720	3	15498.687	16
34.5	14365.062	-7	14318.490	13	15012.657	13	14966.035	-16	15541.970	-12	15495.638	23
35.5	14363.549	-11	14315.654	7			14963.027	-13	15540.164	-14	15492.498	6
36.5	14361.984	-4	14312.756	1	15009.215	17	14959.958	-6	15538.301	-7	15489.310	8
37.5	14360.347	-8	14309.802	-0	15007.369	-5	14956.821	0	15536.374	4	15486.045	1
38.5	14358.647	-13	14306.777	-12	15005.490	7	14953.601	-11	15534.360	-7	15482.706	-16
39.5	14356.895	-7	14303.721	7	15003.527	3			15532.304	8	15479.346	14
40.5	14355.075	-7	14300.574	-3	15001.515	16	14946.997	3	15530.164	3	15475.878	1
41.5	14353.193	-7	14297.375	-4	14999.403	-3	14943.589	4	15527.952	-10	15472.352	-5
42.5	14351.228	-27	14294.125	5	14997.268	24	14940.115	5	15525.683	-15	15468.762	-10
43.5	14349.241	-5	14290.802	3	14995.031	16	14936.572	4	15523.352	-17	15465.093	-31
44.5	14347.175	-2	14287.419	3	14992.723	4	14932.961	1	15520.975	-3	15461.391	-21
45.5	14345.042	-1	14283.971	-1	14990.356	1	14929.280	-4	15518.530	6	15457.647	10
46.5	14342.858	10	14280.476	9	14987.930	6	14925.549	7	15516.007	-2	15453.770	-30
47.5	14340.611	22	14276.913	14	14985.429	5	14921.729	-4	15513.463	31	15449.880	-22
48.5	14338.264	-4	14273.275	6	14982.864	8	14917.860	3	15510.821	25	15445.926	-16
49.5	14335.903	19	14269.580	2	14980.236	16	14913.922	8			15441.929	6
50.5	14333.432	-4	14265.836	10	14977.520	4	14909.904	-1			15437.852	7
51.5	14330.929	3	14262.013	2	14974.742	-1	14905.832	3				
52.5	14328.367	15	14258.128	-7	14971.895	-8	14901.692	7				
53.5	14325.740	25	14254.203	8	14968.982	-12	14897.463	-11				
54.5	14323.029	14	14250.200	5	14966.018	1	14893.210	13				
55.5	14320.249	-3	14246.129	-3	14962.990	19	14888.859	7				
56.5	14317.432	7	14242.005	-2	14959.845	-12	14884.437	-3				
57.5	14314.547	12	14237.820	-0	14956.672	-2	14879.962	2				
58.5	14311.585	4	14233.574	3	14953.416	-6	14875.419	6				
59.5	14308.567	4	14229.260	-0	14950.080	-21	14870.797	-1				
60.5	14305.479	-2			14946.715	2	14866.127	10				
61.5	14302.341	5			14943.246	-8	14861.354	-13				
62.5	14299.114	-13	14215.939	-12	14939.714	-13	14856.540	-11				
63.5	14295.838	-16	14211.390	-0	14936.141	11	14851.660	-6				
64.5	14292.506	-10	14206.765	-1	14932.460	-4	14846.711	-3				
65.5	14289.095	-19	14202.078	-2	14928.727	-2	14841.690	-4				
66.5	14285.641	-8	14197.338	7	14924.918	-7	14836.608	1				
67.5	14282.138	19	14192.500	-18	14921.050	-0	14831.442	-9				
68.5	14278.521	-4	14187.638	-7	14917.115	8	14826.227	0				
69.5	14274.871	5	14182.703	-4	14913.103	9	14820.936	0				
70.5	14271.152	10	14177.700	-6			14815.589	13				

$^4\Phi_{7/2}$ - $^4\Phi_{7/2}$ Sub-band

	0-1				0-0				1-0			
3.5					15022.980a	17			15549.725a	2		
4.5					15023.271a	-65	15016.621a	9	15550.070a	-1	15543.396a	2
5.5					15023.655a	12	15015.579a	4	15550.345a	-4		
6.5					15023.894a	10	15014.476a	5	15550.556a	0	15541.207a	-0
7.5					15024.054a	-4	15013.316a	14	15550.692a	1	15540.119a	111
8.5			14361.541	3	15024.165a	-1	15012.066a	0	15550.759a	4	15538.738a	0
9.5			14360.271	-13	15024.209a	1	15010.768a	4	15550.752a	4	15537.393a	-2
10.5			14358.982	12	15024.182a	-1	15009.397a	1	15550.671a	1	15535.970	-13
11.5	14373.740	15	14357.611	17	15024.087a	-4	15007.976a	15	15550.521a	0	15534.494	-6
12.5	14373.639	8	14356.148	-10	15023.945a	12			15550.304a	4	15532.943	-3
13.5	14373.482	6	14354.674	14	15023.695	-13	15004.895a	3	15550.002a	-6	15531.318	-3
14.5	14373.274	15	14353.097	-3	15023.406	-11	15003.338a	80	15549.650a	5		
15.5	14372.971	-10	14351.474	-6	15023.053	-5	15001.546	-12	15549.212a	2	15527.847	-11
16.5	14372.636	-5	14349.790	-9	15022.609	-24	14999.789	-3	15548.703	-2	15526.027	6
17.5	14372.241	2	14348.056	-1	15022.138	-3	14997.954	-6	15548.124	-3	15524.126	14

TABLE 1—*Continued*

	$^4\Phi_{7/2}$ - $^4\Phi_{7/2}$ Sub-band											
	0-1				0-0				1-0			
J	R(J)	O-C	P(J)	O-C	R(J)	O-C	P(J)	O-C	R(J)	O-C	P(J)	O-C
18.5	14371.776	-0	14346.252	-1	15021.586	3	14996.038	-23	15547.486	7	15522.123	-9
19.5	14371.244	-7	14344.390	2	15020.946	-11	14994.093	-2	15546.746	-13	15520.072	-9
20.5	14370.648	-17			15020.266	0	14992.059	-4	15545.982	15	15517.955	-4
21.5	14370.013	-3	14340.483	8	15019.497	-10	14989.952	-14	15545.093	-12	15515.774	7
22.5			14338.430	4			14987.792	-10	15544.165	-5		
23.5	14368.527	-7	14336.316	-0	15017.792	4	14985.563	-8	15543.160	-4	15511.168	-1
24.5	14367.716	15	14334.155	9	15016.816	-12	14983.266	-8	15542.082	-5	15508.756	-7
25.5	14366.798	-7	14331.922	8	15015.812	11	14980.909	-2	15540.939	3	15506.287	1
26.5	14365.832	-14	14329.616	-4	15014.699	-8	14978.477	-4	15539.719	3	15503.728	-10
27.5	14364.825	-2	14327.264	-1	15013.540	-6			15538.430	7	15501.118	-2
28.5	14363.771	25	14324.849	0	15012.325	8	14973.414	-7	15537.054	-5	15498.427	-3
29.5	14362.598	-4	14322.379	7			14970.786	-5	15535.610	-12	15495.657	-11
30.5	14361.395	-0	14319.828	-4	15009.665	7	14968.083	-12	15534.111	-2	15492.836	-0
31.5	14360.124	-4			15008.222	-7	14965.333	-1	15532.540	7	15489.931	-2
32.5	14358.798	1	14314.574	3	15006.723	-8	14962.514	9	15530.881	0	15486.947	-12
33.5	14357.406	2	14311.839	-9			14959.606	-3	15529.153	-4	15483.898	-16
34.5	14355.964	15	14309.068	5	15003.527	-6	14956.652	5	15527.357	-4	15480.797	1
35.5	14354.427	-5	14306.222	5	15001.831	-1	14953.621	4			15477.614	5
36.5	14352.850	-1	14303.299	-10	15000.060	-5	14950.530	7	15523.543	-9	15474.353	3
37.5	14351.228	18	14300.348	8	14998.219	-10	14947.360	-0	15521.536	-4	15471.047	28
38.5	14349.497	-8	14297.331	22	14996.328	2	14944.123	-7	15519.447	-8	15467.619	0
39.5	14347.744	7	14294.218	2	14994.359	3	14940.829	-6	15517.300	1	15464.149	3
40.5	14345.915	9	14291.063	1	14992.318	2	14937.465	-8	15515.083	12	15460.608	7
41.5	14344.005	-8	14287.843	-3	14990.215	5	14934.043	-0	15512.778	8	15456.992	5
42.5	14342.051	-6	14284.564	-4	14988.040	5	14930.538	-8	15510.385	-11	15453.308	8
43.5	14340.020	-18	14281.224	-5	14985.790	-3	14926.977	-6	15507.952	1	15449.546	4
44.5	14337.959	3	14277.830	3	14983.473	-9	14923.353	0	15505.447	13	15445.715	1
45.5	14335.809	-2	14274.362	-2	14981.108	5	14919.650	-5	15502.846	2	15441.818	4
46.5	14333.598	-4	14270.836	-2	14978.666	11	14915.897	6	15500.197	15	15437.852	10
47.5	14331.346	15	14267.244	-7	14976.139	-0	14912.072	13	15497.445	-3	15433.802	1
48.5	14328.997	0	14263.583	-18	14973.568	12	14908.155	-5	15494.639	-1	15429.678	-8
49.5	14326.603	4	14259.897	7	14970.907	4	14904.197	3	15491.763	1	15425.483	-19
50.5	14324.157	20	14256.127	10	14968.190	8	14900.156	-5	15488.812	1	15421.253	7
51.5	14321.618	5	14252.306	25			14896.058	-2	15485.792	5	15416.914	-6
52.5	14319.017	-7	14248.381	-2			14891.897	5	15482.706	14	15412.529	8
53.5	14316.376	4	14244.425	2			14887.678	20	15479.530	6	15408.060	7
54.5	14313.665	8	14240.413	13			14883.340	-15	15476.277	-7	15403.499	-13
55.5	14310.890	14	14236.314	-1			14878.986	2	15472.967	-5		
56.5	14308.037	4	14232.181	13	14950.409	-3	14874.544	-2	15469.585	-4		
57.5	14305.143	17	14227.972	14	14947.220	11	14870.048	7	15466.131	-1	15389.470	3
58.5	14302.146	-9	14223.679	-6	14943.941	5	14865.452	-15	15462.597	-7	15384.640	-4
59.5	14299.114	-5	14219.346	-4	14940.597	2	14860.833	7	15459.000	-4	15379.758	8
60.5	14296.031	13	14214.958	6	14937.192	8	14856.116	-2	15455.321	-11	15374.777	-8
61.5	14292.860	5	14210.502	11	14933.701	-2	14851.342	1	15451.595	7	15369.748	-2
62.5	14289.619	-7	14205.972	4	14930.162	8	14846.499	3			15364.657	13
63.5	14286.333	1	14201.394	13	14926.509	-26	14841.581	-2			15359.479	11
64.5	14282.968	-7	14196.717	-15	14922.854	9	14836.604	2				
65.5	14279.561	8	14192.018	-1	14919.094	7	14831.555	2				
66.5	14276.079	13	14187.240	-4	14915.254	-3	14826.437	0				
67.5	14272.518	5	14182.408	2	14911.340	-19	14821.257	6				
68.5	14268.877	-19	14177.501	-2	14907.388	-1	14815.999	2				
69.5	14265.227	13	14172.537	-2	14903.333	-17	14810.674	-1				
70.5			14167.502	-8	14899.246	5	14805.288	4				
71.5	14257.644	-10	14162.414	-4	14895.053	-8	14799.824	-1				
72.5	14253.775	-1	14157.272	10	14890.811	0	14794.295	-2				
73.5	14249.838	6	14152.040	-3	14886.484	-6	14788.695	-6				
74.5	14245.836	13	14146.757	-3	14882.090	-7	14783.024	-11				
75.5	14241.756	8	14141.398	-15	14877.626	-9	14777.295	-6				
76.5	14237.610	3	14135.999	-4	14873.095	-7	14771.486	-11				
77.5	14233.402	1	14130.518	-10	14868.493	-4	14765.607	-17				
78.5	14229.128	0	14124.981	-8			14759.674	-9				
79.5			14119.392	5	14859.079	4	14753.675	2				
80.5			14113.735	15	14854.250	-7	14747.590	-2				
81.5			14107.998	9	14849.361	-6	14741.443	0				
82.5			14102.197	4	14844.407	1	14735.232	8				
83.5			14096.348	15	14839.378	5	14728.936	1				
84.5			14090.424	16	14834.273	5	14722.594	17				
85.5							14716.177	28				
86.5												

TABLE 1—*Continued*

$^4\Phi_{9/2}$ - $^4\Phi_{9/2}$ Sub-band												
	0-1				0-0				1-0			
J	R(J)	O-C	P(J)	O-C	R(J)	O-C	P(J)	O-C	R(J)	O-C	P(J)	O-C
12.5					15008.550	-9	14990.950	14				
13.5					15008.356	5	14989.390	15				
14.5	14357.885	1			15008.075	-1	14987.745	-2				
15.5	14357.618	-6					14986.050	-5			15512.111	5
16.5			14334.289	18			14984.298	2	15533.125	-5		
17.5	14356.926	2	14332.536	-2	15006.852	-7	14982.472	-0	15532.566	2	15508.354	-6
18.5	14356.491	9					14980.581	-1	15531.929	2	15506.391	9
19.5	14355.964	-15	14328.879	-12	15005.717	1	14978.631	3	15531.224	6	15504.324	-9
20.5	14355.421	5	14326.979	1	15005.040	-5	14976.600	-7	15530.431	-7	15502.214	1
21.5	14354.794	2	14325.008	5	15004.306	-3	14974.515	-5			15500.023	1
22.5	14354.095	-11	14322.978	10	15003.507	1	14972.370	1	15528.676	11	15497.755	-6
23.5	14353.366	7	14320.859	-14	15002.637	0	14970.153	2	15527.671	0	15495.427	-2
24.5	14352.557	6	14318.727	10	15001.696	-5	14967.861	-7	15526.604	-1	15493.027	1
25.5	14351.679	-2	14316.510	9	15000.702	3	14965.525	6	15525.473	5	15490.545	-7
26.5	14350.749	-1	14314.242	18	14999.628	-2	14963.101	-2	15524.263	4	15488.004	-3
27.5	14349.746	-13	14311.875	-11	14998.501	6	14960.628	5	15522.979	-0	15485.387	-5
28.5	14348.701	-4	14309.487	-2	14997.277	-16	14958.074	-2	15521.627	1	15482.706	1
29.5	14347.600	11	14307.028	-1	14996.029	5	14955.449	-14	15520.207	5	15479.961	14
30.5	14346.418	5	14304.528	19	14994.687	-1	14952.786	2	15518.716	10	15477.125	7
31.5	14345.170	-4	14301.921	-8	14993.290	5			15517.140	3	15474.218	-1
32.5	14343.874	-1	14299.299	12	14991.824	8	14947.220	-9	15515.501	3	15471.238	-8
33.5	14342.500	-13	14296.574	-11	14990.281	1	14944.350	-2	15513.788	3	15468.203	-1
34.5	14341.082	-6	14293.831	10	14988.666	-9	14941.409	0	15511.995	-5	15465.093	2
35.5	14339.601	-1	14291.001	3	14987.008	4	14938.385	-15	15510.150	7	15461.903	-3
36.5	14338.057	3	14288.102	-10	14985.253	-13	14935.325	0			15458.639	-10
37.5	14336.436	-8	14285.169	3	14983.473	12	14932.186	3			15455.321	-0
38.5	14334.771	1	14282.138	-20	14981.588	0	14928.978	4	15504.131	-6	15451.920	-2
39.5	14333.032	-3	14279.087	-2	14979.650	3	14925.689	-10	15501.990	0	15448.454	3
40.5	14331.251	13	14275.953	-5	14977.643	5	14922.360	2	15499.780	9	15444.917	8
41.5	14329.385	6	14272.778	11	14975.562	0	14918.951	1	15497.480	3	15441.288	-7
42.5	14327.446	-9	14269.527	14	14973.414	-3	14915.479	3	15495.108	-3	15437.605	-3
43.5	14325.480	10	14266.199	-0	14971.211	6	14911.934	-0	15492.665	-8	15433.848	-3
44.5	14323.421	-1	14262.836	13	14968.929	4	14908.333	7	15490.170	10	15430.017	-3
45.5	14321.314	4	14259.382	-3	14966.567	-11	14904.655	3	15487.569	-7	15426.122	3
46.5	14319.149	13	14255.902	17	14964.164	4	14900.912	3	15484.919	2	15422.149	4
47.5	14316.902	4	14252.306	-18	14961.660	-16	14897.099	-1	15482.174	-11	15418.100	0
48.5	14314.599	2	14248.703	3	14959.126	3	14893.210	-15	15479.376	-3	15413.974	-8
49.5	14312.233	-1	14245.028	13	14956.494	-7	14889.285	3	15476.498	-3	15409.795	4
50.5	14309.802	-4	14241.270	3	14953.804	-6	14885.270	-1	15473.557	9	15405.520	-9
51.5	14307.325	10	14237.458	0	14951.047	-4			15470.523	2	15401.186	-8
52.5	14304.771	11	14233.574	-12	14948.223	0			15467.424	4		0
53.5	14302.146	4	14229.662	10	14945.322	-3	14872.833	-3	15464.251	5	15392.303	-4
54.5	14299.450	-9	14225.648	-8	14942.359	-1	14868.556	-1	15460.996	-0	15387.759	5
55.5	14296.708	-5	14221.607	10	14939.325	2	14864.220	12	15457.679	5	15383.132	4
56.5			14217.480	4	14936.229	11	14859.800	7	15454.280	4	15378.437	6
57.5			14213.301	9	14933.043	-2	14855.310	1	15450.795	-10	15373.659	-1
58.5			14209.042	-3	14929.797	-4	14850.754	-4	15447.259	1	15368.825	10
59.5			14204.734	-1			14846.140	2	15443.638	1	15363.904	5
60.5	14281.998	-17	14200.383	21	14923.106	3	14841.450	-1	15439.952	10	15358.921	12
61.5	14278.874	-8	14195.930	3	14919.650	0			15436.177	6	15353.841	-5
62.5	14275.691	8	14191.434	6	14916.117	-9	14831.872	1	15432.328	3	15348.718	9
63.5	14272.416	-4	14186.863	-3	14912.538	5	14826.984	6	15428.409	5	15343.501	1
64.5	14269.099	7	14182.242	1	14908.871	2	14822.017	-1	15424.398	-11	15338.214	-2
65.5	14265.701	2	14177.539	-13	14905.127	-7	14816.984	-4	15420.347	10	15332.865	5
66.5	14262.236	-3	14172.806	6	14901.324	-5	14811.886	-4	15416.185	-6	15327.418	-11
67.5	14258.723	8	14167.969	-15	14897.463	10	14806.723	0	15411.965	-3	15321.927	1
68.5	14255.124	-1	14163.113	9	14893.507	0	14801.479	-7	15407.678	7	15316.349	1
69.5	14251.477	8	14158.172	12	14889.495	6	14796.182	0	15403.295	-2	15310.694	-2
70.5	14247.766	19	14153.151	-2	14885.409	9	14790.811	4	15398.850	2	15304.973	2
71.5	14243.956	-3	14148.081	-0			14785.367	4	15394.325	2	15299.183	12
72.5	14240.106	1	14142.946	0			14779.859	9	15389.726	4	15293.292	-6
73.5	14236.195	11	14137.748	2	14872.696	-10	14774.268	-1	15385.036	-9	15287.347	-4
74.5	14232.181	-16	14132.485	3	14868.327	-5	14768.613	-4	15380.280	-11	15281.322	-7
75.5	14228.140	-4	14127.142	-10			14762.895	-0	15375.455	-6	15275.232	-0
76.5	14224.026	3			14859.364	-3			15370.544	-11	15269.056	-6
77.5	14219.826	-10			14854.776	-1	14751.238	-4	15365.578	7	15262.811	-6
78.5	14215.568	-14	14110.787	9	14850.123	8	14745.312	1	15360.514	3	15256.477	-20
79.5	14211.245	-15	14105.199	9	14845.378	-2	14739.300	-9			15250.109	6

TABLE 1—*Continued*

	$^4\Phi_{9/2}$ - $^4\Phi_{9/2}$ Sub-band											
	0-1				0-0				1-0			
J	R(J)	O-C	P(J)	O-C	R(J)	O-C	P(J)	O-C	R(J)	O-C	P(J)	O-C
80.5	14206.865	-7	14099.545	8	14840.571	-2	14733.242	5			15243.639	5
81.5	14202.430	14	14093.823	5	14835.703	11	14727.088	-7				
82.5	14197.887	-4	14088.025	-9	14830.742	3	14720.873	-10				
83.5	14193.294	-6	14082.182	-3	14825.712	-1	14714.598	-1	15334.057	3		
84.5	14188.636	-5	14076.255	-16	14820.625	10	14708.241	-4	15328.541	3		
85.5	14183.911	-2	14070.283	-8	14815.438	-4			15322.945	6		
86.5	14179.123	6	14064.255	11	14810.207	9			15317.273	11		
87.5	14174.270	17	14058.132	-1	14804.877	-2						
88.5	14169.315	-5	14051.936	-18	14799.485	-1						
89.5	14164.312	-7	14045.713	3	14794.023	4						
90.5	14159.245	-5	14039.406	7	14788.479	0						
91.5	14154.102	-9	14033.021	-1	14782.868	4						
92.5	14148.895	-8	14026.564	-14	14777.183	8						
93.5	14143.639	14	14020.057	-11								
94.5	14138.288	9	14013.502	11								
95.5	14132.883	20	14006.835	-12								
96.5			14000.136	0								
97.5			13993.360	3								
98.5			13986.489	-23								
99.5			13979.598	-1								

B

Q-Branch Lines

	$^4\Phi_{3/2}$ - $^4\Phi_{3/2}$				$^4\Phi_{5/2}$ - $^4\Phi_{5/2}$				$^4\Phi_{7/2}$ - $^4\Phi_{7/2}$			
	0-0		1-0		0-0		1-0		0-0		1-0	
J	Obs	O-C	Obs	O-C	Obs	O-C	Obs	O-C	Obs	O-C	Obs	O-C
1.5	15029.522a	2										
2.5	15029.358a	-2	15572.032a	-1	15029.190a	24	15560.856a	5				
3.5			15571.800a	2	15028.940a	4	15560.611a	4	15019.945a	8	15546.720a	1
4.5	15028.853a	1	15571.496a	2	15028.643a	4	15560.290a	-2	15019.647a	9	15546.401a	2
5.5	15028.501a	-1	15571.124a	1	15028.278a	2	15559.911a	2	15019.275a	1	15546.004a	-5
6.5	15028.087a	-1	15570.683a	-1	15027.850a	2	15559.453a	-2	15018.850a	8	15545.553a	6
7.5	15027.618a	7	15570.171a	-7	15027.351a	-3	15558.938a	7	15018.343a	-1	15545.010a	-6
8.5	15027.016a	-5			15026.794a	0	15558.360a	23				
9.5	15026.468a	3	15568.965a	2	15026.164a	-3	15556.943a	2	15017.152a	2		
10.5	15025.798a	1	15568.247a	-8	15025.476a	1	15556.131a	-7				
11.5	15025.059a	-6	15567.484a	6								

Note: "a" marks lines observed in the molecular beam experiments and O-C are observed minus calculated values in units of 10^{-3} cm^{-1}.

for which both laser and FTS measurements are available, only the laser measurements are provided in this table. The rotational lines were weighted according to resolution, extent of blending, and effects of perturbations. Badly blended lines were heavily deweighted. The effective molecular constants for the lower and excited $^4\Phi$ states are provided in Tables 2 and 3, respectively.

At a later stage in the analysis, a spin–orbit interval of 101.84 cm^{-1} was measured between the $X\,^3\Phi_{3/2}$ and $X\,^3\Phi_{5/2}$ spin components from the laser excitation experiments. Therefore, an attempt was made to fit all of the observed lines using the 4×4 matrix appropriate for Hund's case (a) $^4\Phi$ state (Table 4). A free fit of all the subbands was unsuccessful because of the effects of global perturbations. Note the large number of effective rotational constants needed in the excited state in the empirical analysis (Table 3). The ground state case (a) rotational constants, however, were determined from a fit of the combination differences. In this fit the spin–orbit parameter A was fixed to 33.95 cm^{-1}, a value determined from the observed spacing of 101.84 cm^{-1} ($3A$) between

TABLE 2
Effective Molecular Constants (in cm^{-1}) for the $X^4\Phi$ State of TiF

	$X^4\Phi_{3/2}$		$X^4\Phi_{5/2}$	
Const.[a]	v=0	v=1	v=0	v=1
T_{vv}	0.0	650.6136(20)	0.0	650.6801(21)
B_v	0.3647520(79)	0.3622256(86)	0.3669854(99)	0.3644512(99)
$10^7 \times D_v$	4.2524(86)	4.198(14)	4.462(16)	4.476(16)
	$X^4\Phi_{7/2}$		$X^4\Phi_{9/2}$	
Const.	v=0	v=1	v=0	v=1
T_{vv}	0.0	650.7360(16)	0.0	650.7782(18)
B_v	0.3693793(77)	0.3668046(77)	0.3718279(64)	0.3692221(62)
$10^7 \times D_v$	4.8129(91)	4.8064(90)	5.1450(61)	5.1407(58)

[a]The numbers in parentheses are one standard deviation in last two digits.

the 3/2 and 5/2 spin components. The case (a) molecular constants for $v = 0$ of the $X^4\Phi$ state are provided in Table 5. In this fit only lines with $J \leqslant 30.5$ were used and the RMS error of the fit was 0.008 cm^{-1}. When the range of J was extended, the quality of the fit deteriorated.

DISCUSSION

Prior to the present work very limited spectroscopic information was available for TiF. The initial theoretical study of TiF by Cambi (*36*) is not very reliable. A reliable prediction of the spectroscopic properties of TiF requires the use of high-level ab initio calculations with large basis sets and extensive electron correlation. A recent calculation by Harrison (*38*) is a giant step forward, at least for the low-lying states.

In our previous studies of transition metal fluorides and hydrides we have noted a close similarity between the electronic transitions. A detailed comparison for the CoH/CoF, FeH/FeF, and ScH/ScF pairs has been reported previously (*28–30*). It has been concluded that the low-lying electronic states of transition metal hydrides, *M*H, and fluorides, *M*F, also correlate directly with the states of the M^+ atom. There is a very high-quality set of ab initio calculations for TiH (*35*) which can be compared with the available results for TiF (*38*). The correlation diagram of the electronic states of TiF, TiH, and Ti^+ provided in Fig. 6 suggests that their energy levels share a remarkably similar pattern. The F^- and H^- ligands give rise to similar energy level patterns in TiF and TiH, although the bonding in TiH is expected to be much more covalent than that in TiF.

The lowest energy term of the Ti^+ atom is a^4F which arises from the $3d^24s^1$ configuration (*46*). This ^4F term correlates to the $X^4\Phi$, $A^4\Sigma^-$, $B^4\Pi$, and $C^4\Delta$ states in TiH and TiF (Fig. 6). The first excited term in Ti^+ is b^4F at $\sim$1000 cm^{-1}, arising from the $3d^3$ configuration (*46*). The TiF and TiH molecular states correlating to b^4F are $^4\Sigma^-$, $^4\Delta$, $^4\Phi$, and $^4\Pi$ (Fig. 6). From Fig. 6 it appears that the general picture of the low-lying states of TiH and TiF can be predicted from the Ti^+ energy levels, although the ordering of states corresponding to a particular atomic term is difficult to predict and may change on going from hydride to fluoride. The third Ti^+ term, a^2F ($3d^24s^1$), at 4700 cm^{-1}, correlates with the $a^2\Delta$, $b^2\Pi$, $c^2\Phi$, and $d^2\Sigma^-$ states of TiH.

The detailed energy ordering as presented in Fig. 6 is probably not completely correct. However, we are sufficiently confident of the qualitative correctness of Fig. 6 that we use the letter labels $G^4\Phi-X^4\Phi$ for our new transition. The ground $X^4\Phi$ electronic state of TiF is derived from the metal-centered $\sigma^1\pi^1\delta^1$ configuration. According to the theoretical predictions of Harrison (*38*), the lowest excited quartet state is the $A^4\Sigma^-$ state, located at 0.1 eV. This state arises from the $\sigma^1\delta^2$ configuration. The next higher excited states, $B^4\Pi$ and $C^4\Delta$, arise from $\sigma^1\pi^1\delta^1$ and $\pi^2\delta^1$ configurations, respectively. There are two low-lying metal-centered σ orbitals (nominally $4s\sigma$ and $3d\sigma$) and the $G^4\Phi-X^4\Phi$ tran-

TABLE 3
Effective Molecular Constants (in cm^{-1}) for the $G^4\Phi$ State of TiF

	$G^4\Phi_{3/2}$		$G^4\Phi_{5/2}$	
Const.[a]	v=0	v=1	v=0	v=1
T_{vv}	15029.63865(41)	15572.32890(61)	15029.45439(57)	15561.15633(69)
B_v	0.3329530(80)	0.3310104(99)	0.334039(10)	0.332085(11)
$10^7 \times D_v$	5.7585(97)	4.335(78)	5.047(22)	4.902(62)
$10^{12} \times H_v$	3.617(68)	21.1(34)	0.64(18)	66.8(19)
$10^{14} \times L_v$	--	1.219(44)	--	--
	$G^4\Phi_{7/2}$		$G^4\Phi_{9/2}$	
Const.	v=0	v=1	v=0	v=1
T_{vv}	15020.45911(72)	15547.27716(63)	15004.9369(13)	15531.5592(19)
B_v	0.3362104(77)	0.3339075(83)	0.3390850(64)	0.3365450(69)
$10^7 \times D_v$	5.3326(90)	5.452(26)	6.0019(68)	6.049(10)
$10^{12} \times H_v$	--	6.32(47)	0.561(26)	1.405(72)

[a]The numbers in parentheses are one standard deviation in last two digits.

sition results from shifting an electron from the lower energy σ orbital to the higher σ orbital.

The ground state of TiH is known to be $X\,^4\Phi$ on the basis of both experimental observations (*32–34*) and theoretical calculations (*35*). However, there has been controversy over the nature of the ground electronic state of TiF (*17, 18, 38*). The early low-resolution work on TiF by Diebner and Kay (*17*) and Chatalic *et al.* (*18*) suggested a $^4\Sigma^-$ ground state, supported by the prediction of Cambi (*36*). In contrast to this, another study of the TiF molecule at grating resolution by Shenyavskaya *et al.* (*19*) favors a $^2\Delta$ ground state. The most recent theoretical prediction on TiF by Harrison (*38*), however, predicts a $^4\Phi$ ground state. This assignment is also consistent with the results available for TiH, from both experimental (*32–34*) and theoretical studies (*35*).

A comparison of the rotational constants of Shenyavskaya *et al.* (*19*) with the values obtained in the present work indicates that their $v = 0$ $^2\Delta_{3/2}$ rotational constants agree very well with our constants for $v = 0$ of the $^4\Phi_{3/2}$ spin component. This indicates that their $^2\Delta_{3/2}$ state is most probably the $X\,^4\Phi_{3/2}$ spin component. However, there seems to be some problems in their analysis of the bands involving $v'' = 1$ since their constants for $v'' = 1$ and their value of $\Delta G''(1/2) = 675$ cm^{-1} do not agree with the corresponding values obtained in this work. We note that the visible spectra are extremely complicated and several of the observed bands (which could be the missing spin components) were left unassigned.

The $\Delta G(1/2)$ values of the four spin components $X\,^4\Phi_{3/2}$ (650.61 cm^{-1}), $X\,^4\Phi_{5/2}$ (650.68 cm^{-1}), $X\,^4\Phi_{7/2}$ (650.74 cm^{-1}), and $X\,^4\Phi_{9/2}$ (650.78 cm^{-1}) are nearly identical, consistent with a well-behaved case (*a*) $^4\Phi$ state. A similar comparison of the excited state vibrational intervals for $G^4\Phi_{3/2}$ (542.69 cm^{-1}), $G^4\Phi_{5/2}$ (531.71 cm^{-1}), $G^4\Phi_{7/2}$ (526.82 cm^{-1}), and $G^4\Phi_{9/2}$ (526.62 cm^{-1}) shows the effects of strong interactions with other states.

Since the constants for the four spin components of the $^4\Phi$ states have been determined by treating each spin component as an individual state, the determination of ''true'' Hund's case (*a*) constants from the effective constants is necessary. A simple perturbation theory analysis of the 4×4 matrix representation of the energy levels of a $^4\Phi$ state leads to the following relationships:

$$B_{\text{eff}}(3/2) = B(1 - B/A) \quad [2a]$$

$$B_{\text{eff}}(5/2) = B(1 - B/3A) \quad [2b]$$

$$B_{\text{eff}}(7/2) = B(1 + B/3A) \quad [2c]$$

TABLE 4
Matrix Elements for a Hund's Case (*a*) $X^4\Phi$ state[a,b]

	$\|^4\Phi_{9/2}\rangle$	$\|^4\Phi_{7/2}\rangle$	$\|^4\Phi_{5/2}\rangle$	$\|^4\Phi_{3/2}\rangle$
$\langle^4\Phi_{9/2}\|$	T_0+9/2 A+3γ + (B + 9/2 A_D) (x - 19) - D(x^2 - 35x + 313)	√3(B - γ + 6A_D)(x -16)$^{1/2}$ - (12)$^{1/2}$D(x -16)$^{1/2}$(x-19)	-4√3D(x^2 - 25x +144)	0
$\langle^4\Phi_{7/2}\|$		T_0 +3/2 A - 2γ + (B +3/2 A_D) (x - 9) - D(x^2 - 11x - 3)	2(B - γ)(x - 9)$^{1/2}$ - 4D(x - 9)$^{1/2}$ (x - 6)	-4√3D(x^2 - 13x +36)
$\langle^4\Phi_{5/2}\|$			T_0 -3/2 A - 5γ + (B - 3/2 A_D) (x - 3) - D(x^2 + x - 39)	√3(B - γ - A_D)(x - 4)$^{1/2}$ - (12)$^{1/2}$D(x - 4)$^{1/2}$(x - 4)
$\langle^4\Phi_{3/2}\|$	symmetric			T_0 - 9/2 A - 6γ + (B - 9/2 A_D) (x - 1) - D(x^2 + x - 11)

[a] $x = (J + 1/2)^2$

[b] The matrix elements listed in this table are derived from the general Hund's case (a) matrix elements given by Zare et al. (47).

$$B_{\text{eff}}(9/2) = B(1 + B/A). \qquad [2d]$$

TABLE 5
Case (*a*) Molecular Constants for the $X^4\Phi$ Ground State of TiF

Constant	Value (cm^{-1})
A	33.95[a]
$10^4 \times A_D$	7.64[b]
B	0.368173(27)[c]
$10^7 \times D$	4.03(22)
γ	0.347(13)

[a] Fixed at the value determined by the spin–orbit spacing of the 3/2 and 5/2 spin components, $3A$ = 101.84 cm^{-1}, ignoring the small contribution of γ, as determined in the laser excitation experiments.

[b] Fixed at the value as determined from a fit only to the molecular beam data. Including the FTS data gave a strong degree of correlation between γ and A_D.

[c] The numbers in parentheses are one standard deviation in the last digits.

In these equations A is the usual spin–orbit coupling constant and B is the ''true'' rotational constant associated with the $^4\Phi$ state. A quick check using Eqs. [2a]–[2d] leads to the conclusion that both the $G^4\Phi$ and $X^4\Phi$ states are regular ($A > 0$). Equations [2a]–[2d] work surprisingly well considering that the subband origins are spaced so irregularly. For example, for $v = 0$ in the $X^4\Phi$ state $B_{\text{eff}}(5/2) - B_{\text{eff}}(3/2) = 0.002233$ cm^{-1}, $B_{\text{eff}}(7/2) - B_{\text{eff}}(5/2) = 0.002394$ cm^{-1}, and $B_{\text{eff}}(9/2) - B_{\text{eff}}(7/2) = 0.002449$ cm^{-1} which gives $B_0'' = 0.3682$ cm^{-1} and $A_0'' = 38$ cm^{-1} by simple averaging. For the excited $G^4\Phi$ state $B_0' = 0.3356$ cm^{-1} and $A_0' = 37$ cm^{-1}. The spin–orbit intervals ($3A$) are thus about 114 cm^{-1} in the $X^4\Phi$ state and about 111 cm^{-1} in the $G^4\Phi$ state. The observed 3/2–5/2 ground state spin–orbit interval of 101.84 cm^{-1} and the Hund's case (*a*) B'' value of 0.368173 (27) cm^{-1} (Table 5) are in excellent agreement with the corresponding values extracted from the empirical constants.

The equilibrium internuclear separation r_e was found by using effective B_0 and B_1 values for each spin component to calculate effective B_e values and then averaging them to obtain a ''true'' B_e value. Using this algorithm for the $X^4\Phi$

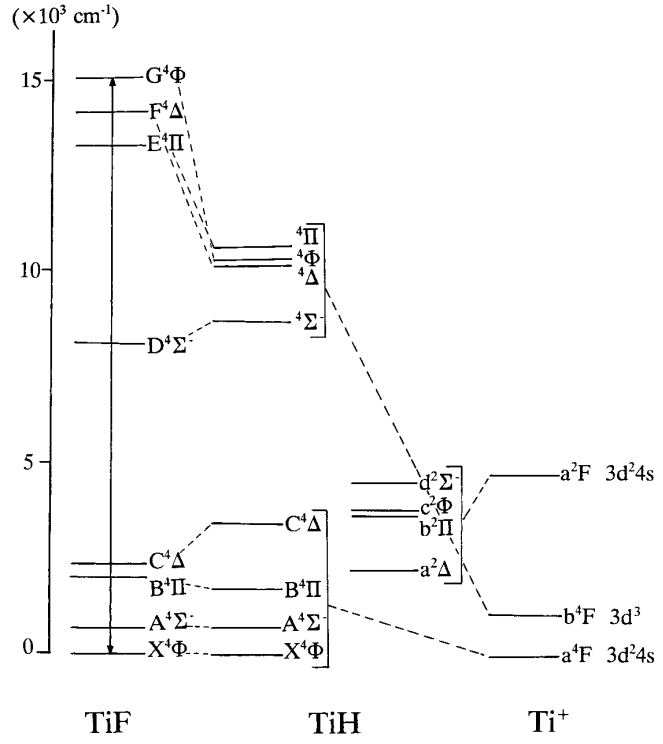

FIG. 6. A correlation diagram of the electronic energy levels of TiF (*38*) and TiH (*35*) with the atomic energy levels of Ti^+ (*46*). The energy levels of TiH are obtained by ab initio calculations (*35*) while those for TiF are based partly on ab initio calculations (*38*) and partly on our empirical estimates. The observed transition of TiF has been marked with a double arrow and the position of the $G^4\Phi$ state of TiF has been taken from the present work.

state gives $B_e = 0.3695\ cm^{-1}$, $\alpha_e = 0.0026\ cm^{-1}$, and $r_e = 1.8311$ Å, while for the $G^4\Phi$ state the values are $B_e = 0.3367\ cm^{-1}$, $\alpha_e = 0.0022\ cm^{-1}$, and $r_e = 1.9192$ Å. Averaging the $\Delta G(1/2)$ values results in $\Delta G''(1/2) = 650.70\ cm^{-1}$ and $\Delta G'(1/2) = 532\ cm^{-1}$.

CONCLUSIONS

The emission spectrum of TiF has been observed at high resolution using a Fourier transform spectrometer as well as by laser excitation spectroscopy. Three bands in the region 13 500–16 000 cm^{-1}, with heads at 14 388, 15 033, and 15 576 cm^{-1}, have been assigned as the 0–1, 0–0, and 1–0 vibrational bands of a new $G^4\Phi$–$X^4\Phi$ transition. A rotational analysis of these bands has been carried out and the molecular constants have been determined. The lower $^4\Phi$ state has been assigned as the ground state of TiF consistent with the theoretical predictions of Harrison (*38*) and expectations based on the available information for TiH (*32–35*). The ground state is a relatively well-behaved case (*a*) $^4\Phi$ state with $\Delta G(1/2) = 650.70\ cm^{-1}$ and $r_e = 1.8311$ Å. The $G^4\Phi$–$X^4\Phi$ transition is analogous to the 1-μm transition of TiH (*42*). The similarity between the electronic energy levels of TiF, TiH, and Ti^+ has been discussed. More work, both experimental and theoretical, is necessary to straighten out the spectroscopy of the titanium, zirconium and hafnium monohalides. We have already started on this task by recording new infrared and near-infrared spectra of TiCl and ZrCl.

ACKNOWLEDGMENTS

We thank J. Wagner and C. Plymate of the National Solar Observatory for assistance in obtaining the spectra. The National Solar Observatory is operated by the Association of Universities for Research in Astronomy, Inc., under contract with the National Science Foundation. The research described here was supported by funding from the NASA laboratory astrophysics program. Support was also provided by the Petroleum Research Fund administered by the American Chemical Society and the Natural Sciences and Engineering Research Council of Canada. We thank J. Harrison for providing the results of his calculations prior to publication.

REFERENCES

1. C. Jascheck and M. Jascheck, ''The Behavior of Chemical Elements in Stars,'' Cambridge Univ. Press, Cambridge, 1995.
2. P. W. Merrill, A. J. Deutsch, and P. C. Keenan, *Astrophys. J.* **136,** 21–34 (1962).
3. G. W. Lockwood, *Astrophys. J. Suppl.* **24,** 375–420 (1972); *Astrophys. J.* **180,** 845–855 (1973).
4. M. Grunze, *in* ''The Chemical Physics of Solid Surfaces and Heterogeneous Catalysis'' (D. A. King and D. P. Woodruff, Eds.), Vol. 4, p. 143, Elsevier, New York, 1982.
5. F. A. Cotton and G. Wilkinson, ''Advanced Inorganic Chemistry. A Comprehensive Text,'' 5th ed., Wiley, New York, 1988.
6. M. Freindorf, C. M. Marian, and B. A. Hess, *J. Chem. Phys.* **99,** 1215–1223 (1993).
7. S. R. Langhoff and C. W. Bauschlicher, Jr., *J. Mol. Spectrosc.* **141,** 243–257 (1990).
8. C. W. Bauschlicher, Jr., and P. Maitre, *Theor. Chem. Acta* **90,** 189–203 (1995).
9. R. E. S. Clegg, D. L. Lambert, and R. A. Bell, *Astrophys. J.* **234,** 188–199 (1979).
10. G. E. Hale, W. S. Adams, and H. G. Gale, *Astrophys. J.* **24,** 185–218 (1906).
11. H. Wöhl, *Solar Phys.* **16,** 362–372 (1971).
12. Engvold, *Astron. Astrophys. J. Suppl.* **10,** 11–16 (1973).
13. R. Yerle, *Astron. Astrophys.* **73,** 346–353 (1979).
14. A. J. Cernicharo and M. Guélin, *Astron. Astrophys.* **183,** L10–L12 (1987).
15. L. M. Ziurys, A. J. Apponi, and T. G. Phillips, *Astrophys. J.* **433,** 729–732 (1994).
16. A. Jorisson, V. V. Smith, and D. L. Lambert, *Astron. Astrophys.* **261,** 164 (1992).
17. R. L. Diebner and J. G. Kay, *J. Chem. Phys.* **51,** 3547–3554 (1969).
18. A. Chatalic, P. Deschamps, and G. Pannetier, *C. R. Acad. Sci. Paris,* **270,** 146–149 (1970).
19. E. A. Shenyavskaya, Y. Y. Kuzyakov, and V. M. Tatevskii, *Opt. Spectrosc.* **12,** 197–199 (1962).
20. A. Chatalic, P. Deschamps, and G. Pannetier, *C. R. Acad. Sci. Paris,* **268,** 1111–1113 (1969).
21. T. C. DeVore, *High Temp. Sci.* **15,** 263–273 (1982).

22. A. Chatalic, P. Deschamps, and G. Pannetier, *J. Chim. Phys.* **67,** 316–322 (1970).
23. C. Sivaji and P. T. Rao, *J. Phys. B* **3,** 720–724 (1970).
24. C. Sivaji, D. V. K. Rao, and P. T. Rao, *Curr. Sci. (India)* **39,** 153–154 (1970).
25. K. D. Carlson and C. Moser, *J. Chem. Phys.* **44,** 3259–3265 (1966).
26. E. A. Shenyavskaya and V. M. Dubov, *J. Mol. Spectrosc.* **113,** 85–92 (1985).
27. J. G. Phillips and S. P. Davis, Astr. Phys. J. Suppl. Ser. **71,** 163–172 (1989).
28. R. S. Ram, P. F. Bernath, and S. P. Davis, *J. Chem. Phys.* **104,** 6949–6955 (1996).
29. R. S. Ram, P. F. Bernath, and S. P. Davis, *J. Mol. Spectrosc.* **179,** 282–298 (1996).
30. R. S. Ram and P. F. Bernath, *J. Mol. Spectrosc.* (in press).
31. R. S. Ram, P. F. Bernath, and S. P. Davis, *J. Mol. Spectrosc.* **175,** 1–6 (1996).
32. A. G. Gaydon, *J. Phys. B* **7,** 2429–2432 (1974).
33. T. C. Steimle, J. E. Shirley, B. Simard, M. Vasseur, and P. Hackett, *J. Chem. Phys.* **95,** 7179–7182 (1991).
34. O. Launila and B. Lindgren, *J. Chem. Phys.* **104,** 6418–6422 (1996).
35. J. Anglada, P. J. Bruna, and S. D. Peyerimhoff, *Mol. Phys.* **69,** 281–303 (1990).
36. R. Cambi, *Gazz. Chim. Ital.* **105,** 27–35 (1975).
37. R. F. Fenske, K. G. Caulton, D. D. Radtke, and C. C. Sweeney, *Inorg. Chem.* **5,** 951–960 (1966).
38. J. F. Harrison, private communication.
39. K. F. Zmbov and J. L. Margrave, *J. Phys. Chem.* **71,** 2893–2894 (1967).
40. V. M. Petrov, G. V. Girichev, K. S. Krasnov, and E. Z. Zasorin, *Zh. Strukt. Khim.* **20,** 55–59 (1979).
41. T. C. DeVore, R. J. Van Zee, and W. Weltner, Jr., *in* ''Proceedings, Symposium on High Temperature Halide Chemistry'' (D. L. Hildenbrand and D. D. Cubicciotti, Eds.), Vol. 78-1, pp. 187–198, 1978.
42. R. S. Ram and P. F. Bernath, unpublished.
43. A. G. Adam, L. P. Fraser, W. D. Hamilton, and M. C. Steeves, *Chem. Phys. Lett.* **230,** 82–86 (1994).
44. A. G. Adam and J. R. D. Peers, *J. Mol. Spectrosc.* **181,** 24–32 (1997).
45. S. Gerstenkorn and P. Luc, ''Atlas du Spectre d'Absorption de la Molecule d'Iode,'' Laboratoire Aimé Cotton, CNRS 91405, Orsay, France, 1978.
46. C. E. Moore, ''Atomic Energy Levels,'' Vol. I, Natl. Bur. of Standards, Washington, DC, 1949.
47. R. N. Zare, A. L. Schmeltekopf, W. J. Harrop, and D. L. Albritton, *J. Mol. Spectrosc.* **46,** 37–66 (1973).